 doi:10.20944/preprints202209.0108.v1

Article

Selection of CMIP6 Climate Models Using Statistical and Data Mining Approaches, Case of Upper Awash Sub-Basin (UASB), Ethiopia

Yonas Balcha [1,‡,*] 0000-0001-9016-0494, Andreas Malcherek [2,‡] and Tena Alamirew [3,†]

[1] Universität der Bundeswehr München, Department of Civil Engineering and Environmental Sciences, Werner Heisenberg Weg-39, Neubiberg; yonabe2001@gmail.com; yonas.balcha@unibw.de
[2] Universität der Bundeswehr München, Department of Civil Engineering and Environmental Sciences, Werner Heisenberg Weg-39, Neubiberg; andreas.malcherek@unibw.de
[3] Ethiopian Water Resources Institute, Water and Land Resource Center Addis Abab University, Addis Ababa; alamirew2004@yahoo.com
* Correspondence: yonabe2001@gmail.com

Abstract: Climate change is a phenomenon that makes the climate system of a given region to be more unpredictable and increases the risk of water-related problems. GCMs under the new CMIP6 framework holds several climate models with many improvements as compared to past similar efforts. The improvements are mainly in the number of scenarios formulated, setup, parametrization, and resolution. In this study, 10 downscaled climate models from CMIP6 are evaluated by applying statistical and data mining tools and are ranked based on their capability to describe the historical observed series. The result of the analysis showed that the outputs of the MPI-ESM1-2-HR model have a good overall ranking among those 10 models. The output of this top-ranked model is used to understand future climate over UASB after properly bias-corrected using the QM method. Results of the bias correction step show that average annual precipitation has shown an increment of 6.5% in the middle (SSP2-4.5) and 10.3% in the worst (SSP5-8.5) case scenarios for the mid-century (2040 - 2069). Similarly, for the end of the century (2070 - 2099) an increment of 4.7% and 17.5% was predicted for the two scenarios respectively. Whereas average annual maximum temperature series showed an increment of 1.5 $^{\circ}C$ for middle and 2.6 $^{\circ}C$ for the worst case in the mid-century. At the same time, an increment of 2.2 $^{\circ}C$ and 3.5 $^{\circ}C$ were predicted for the end of the century similarly for those scenarios. Furthermore, it was predicted that the average annual minimum temperature series will have an increment of 2.6 $^{\circ}C$ and 3.1 $^{\circ}C$ for mid-century and 3.1 $^{\circ}C$ and 4.7 $^{\circ}C$ for the end century for the two scenarios respectively. An increase in precipitation with increased land degradation problems in the sub-basin increases the risk of flood events in the future.

Keywords: GCMs; PDF; Trend Test ; IDW; QM; PCA; DTW; Biascorrection; Ethiopia; climate change

1. Introduction

Securing water that satisfies every human need is the main priority and still a challenge to date being faced by many countries throughout the world. Socio-economic growth, changing consumption patterns, and population growth are thought to be the main driving factors for the ever-increasing water demand [1]. The global freshwater composition which is accessible to a human being is less than 1% which makes it a limited resource [2]. In addition, the natural uneven distribution of rainfall globally further adds to the complexity of making this resource accessible in adequate amount to all.

Aside from the natural variation in rainfall distribution, since the past few decades, it is being contemplated that climate change is further contributing to this variability [3]. This artificial climate variability is manifesting itself as droughts and floods in different parts of the world. Two recent phenomena that support this point are the flood events in

 doi:10.20944/preprints202209.0108.v1

Mecca, Saudi Arabia in April 2021 [4] and the drought event in southeastern Alaska, the USA in July, 2019 [5].

According to a study done by NMA (National Metrological Agency) on climate change adaptation, the major impacts of climate variability in Ethiopia are food insecurity, outbreaks of water-borne diseases, land degradation, and damage to infrastructure [6]. Particularly Awash basin is a basin that supports a huge population since it holds several major cities and towns including the capital city Addis Ababa [7]. The basin is one of the highly utilized basins in the country in terms of water use mainly for irrigation purposes. Most of the irrigation is practiced in the middle and lower part of the basin. In addition, intensive rain-fed agriculture dominates the upper basin areas [8,9]. This part of the basin is mostly highland and is densely populated as compared to the middle and lower part of the basin.

Awash River is the major river that drains the Awash basin and a large proportion of its average annual flow comes from the upper basin areas. This is due to a relatively high average annual precipitation that falls on these parts of the basin [10]. In recent years, water security issues are becoming more evident. This is due to the occurrence of more frequent flood and drought events especially in the middle and lower parts of the basin [11,12].

One of the widely used techniques in studying the impacts of climate change on the water resource of a given place is through the use of outputs from Global Climate Models (GCMs). GCMs are mathematical equations that describe the global climate system with three-dimensional grids and are used to simulate the effect of greenhouse gas emissions on climate [13]. It is undeniable that since their introduction, the outputs from GCMs have been essential in understanding the past, current, and future climate of the earth. The use of GCMs is often limited to global or regional scales mainly due to their coarse resolution. However, with a proper application of a combination of downscaling and bias correction techniques, GCMs can be useful in understanding the local climate and play a vital role in decision making process for water resource planning and management [14,15].

In recent years the challenge in predicting future climate is not not only focused on climate modeling but also how to use them. This is due to the sheer number of climate model outputs currently available worldwide. As a result, often models have to be evaluated for their performance in simulating the climate characteristic of the area in which they are to be applied. The criteria to be used for climate model evaluation is dependent on the goal of climate model selection [16].

There are different versions and experiments of climate models generated at different institutions and locations throughout the world. This makes the inter-comparison between models highly cumbersome. This is the reason behind the establishment of CMIP with the intention of putting the various model development efforts throughout the world by different institutions into one framework [17]. Currently, new sets of models belonging to sixth CMIP framework have been released. The main difference between models released at each stage of the framework is mainly improvements in the model setup, resolution, scenarios, and parametrization [18].

The CMIP6 archive currently holds model output results from more than 30 climate research centers found on different continents throughout the globe [17]. Each model which comes from these centers is different, because of this the outputs generated for the same experiment and scenario are different [19]. As a result, not all models perform well in a certain location. And this is why there is a need to evaluate the capabilities of models and select those which have better performance in describing the local climate is required [16,20].

In practice, one climate model or a small ensemble of climate models are selected for climate change impact studies. In most cases, the selection could be based on a single criterion or a whole set of criteria. Climate models are often selected based on their skill to simulate the present and near past climate. This approach is known as Past–Performance Approach. Another one is called Envelop Approach where an ensemble of models covering

 doi:10.20944/preprints202209.0108.v1

a wide range of projections for one or more climate variables of interest is selected from the pool of available models [16,21].

Up to know there is no clearly defined methodology to be used for evaluating and selecting a single or group of climate models. The selection method and process mainly depend on the aim of the study and the variables involved [16]. Most of the works which have been done so far use statistical or data mining techniques. Also, there is a difference in the output (single or ensemble model), Analysis period (daily, monthly, seasonal, and Annual), and level (station, grid, regional, or spatial averaged).

The most common statistical techniques applied for evaluation of climate models are Performance indicators, Descriptive Statistics, and indices [22–25]. Aside from this data mining methods such as Singular Value Decomposition (SVD), Principal Component Analysis (PCA), Hierarchical Clustering, Symmetrical Uncertainty (SU), and Canonical Correlation Analysis (CCA) are also applied [20,21,26–29]. Using a combination of these various techniques instead of a single method helps not only in reducing the uncertainty of wrong selection but also improves it by including various characteristics of the time series. Techniques that are often used and help in incorporating multiple selection methods are Skill Score (SS) and Multi-Criteria Decision Analysis (MCDA) [16,30].

In the past, there were few attempts which aimed at understanding the climate of the Awash basin at large and the Upper-Awash basin in particular. One of the earliest works on the Awash basin was by [31] where the outputs from three randomly selected GCMs (CCCM, GFD3, and GFDL) together with two scenarios were used in predicting a future runoff condition. After evaluating the potential of GCMs for their annual cycle, seasonal biases, variability, and trend three CMIP5 GCMs were selected and used for studying the impact of climate change by [32]. The impact of climate change on the river basin was studied with help of a few selected models from the CMIP5 archive for different scenarios identified from previous works [33]. Similarly, an ensemble of two GCMs [34] and three selected GCMs [35] from the CMIP5 archive was used to characterize the river flow in the first case and to estimate river nutrient load in the second one. Ensemble mean of five randomly selected GCMs from the CMIP5 archive was used in characterizing the hydro-meteorological situation in the Upper-Awash Basin by [36]. Most recently similar research which was published also suggests a group of four climate models which come from different ensembles of the CMIP6 climate model as an output [37]. Two approaches that combine envelop and past performance approach are put to use in evaluating outputs of CMIP6 after [16].

Previous climate model selection efforts undertaken so far have not evaluated climate models thoroughly for their capability to simulate the climate system over UASB. Therefore, in this study, more robust approaches which mainly rely on statistical and data mining techniques are proposed to evaluate the climate model outputs from the new CMIP6. The result of the selection process would enable us to answer two main questions: 1) Which climate model can better simulate the climate over UASB? And 2) What could be expected in terms of future climate over the basin?

2. Materials and Methods

2.1. STUDY AREA AND DATA USED

The study is focused on the Upper Awash sub-basin which is found in central Ethiopia and is located between a longitude of $37°57'4''E - 39°17'28''E$ and a latitude of $8°4'52''N - 9°19'47''N$. The basin has a total drainage area of 12043 km^2 and contributes the majority of the annual flow to the larger Awash Basin. The mean annual precipitation ranges from 861 mm to 1223 mm at Boneya and Addis Ababa respectively. And the mean annual temperature is in the range of $17°C$ at Addis Ababa to $21°C$ in Melkasa. The topography of the drainage basin ranges from 3561 m in altitude near ArbGebya and as low as 1547 m at Koka lake.

Preprints (www.preprints.org) | NOT PEER-REVIEWED | Posted: 7 September 2022 doi:10.20944/preprints202209.0108.v1

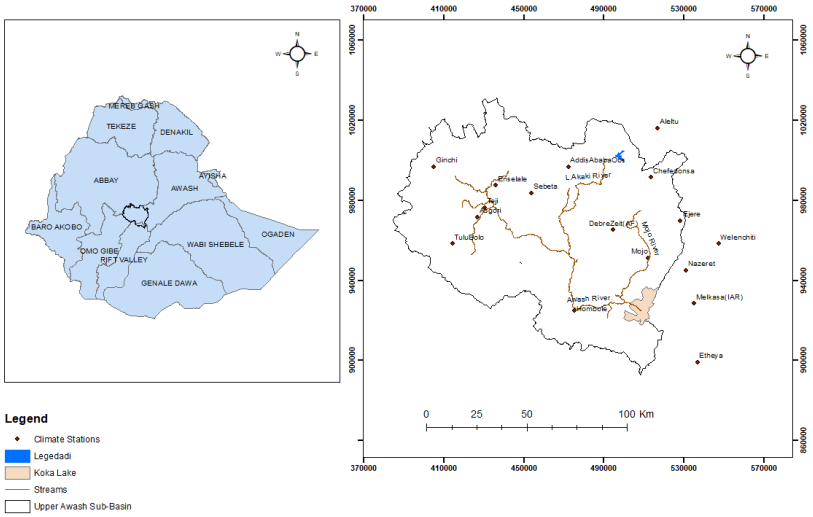

Figure 1. Map of Upper Awash Sub-Basin with major rivers and location of metrological stations.

For the climate model evaluation a total of 15 rainfall and 10 temperature stations are used. The list of stations used is shown in the Table 1 below.

Table 1. List of metrological stations in the Upper Awash Sub-Basin used for analysis.

No.	Station Name	Location (y)	Location (x)	Altitude
1	Addis Ababa Obs*	472248.08	996952.4	2386
2	Addis Alem**	432225.93	999552.91	2372
3	Aleltu	516771.63	1016119.33	2648
4	Ambo**	372449.79	993358.73	2068
5	Asgori*	426775.97	971700.31	2072
6	Boneya	460591.24	971046.06	2251
7	Bui**	450940.01	920899.89	2054
8	ChefeDonsa	513542.53	991537.73	2392
9	Debrezeit*	494500.33	965370.79	1900
10	Ejere	528246.66	969798.67	2254
11	Enselale	435870.79	987532.37	2000
12	Ginchi	404738.43	996808.09	2132
13	Hombole	475209.16	925006.74	1743
14	Huruta*	537697.21	900012.17	2044
15	Melkasa*	534861.76	928532.98	1540
16	Mojo	511901.68	951220.7	1763
17	Nazret	531179.91	945113.49	1622
18	Sebeta	459322.66	986027.98	2220
19	Teji	430354.91	976481.48	2091
20	Tulu Bolo*	414188.26	958456.67	2100
21	Welenchiti	547305.49	958395.38	1458
22	Woliso**	388113.76	945249.62	2058

N.B: ** are only used for temperature stations and * are for both.

Overall 10 climate models were preliminary identified from the WCRP CMIP6 archive (https://esgf-node.llnl.gov/search/cmip6/) to be used for the study based on model availability for all variables (Precipitation, Tmax and Tmin) for the historical time period. The criteria used to filter the models is daily data, 100 km nominal resolution, source type:

 doi:10.20944/preprints202209.0108.v1

AOGCM and from r1i1p1f1 variant. The models were accessed from this site on August 17,2021. The list of models used for analysis is shown in the Table 2.

Table 2. List of candidate climate models used in the selection process

Data Type	Institute	Country
MRI-ESM2-0	Meteorological Research Institute	Japan
ECEARTH3-CC	EC-Earth consortium	Sweden
NorESM2-MM	Norwegian Climate Center	Norway
TaiESM1	Academia Sinica	Taiwan
ECEARTH3.Veg	EC-Earth consortium	Sweden
MPI-ESM1.2.HR	Max Planck Institute for Meteorology	Germany
ECEARTH3	EC-Earth consortium	Sweden
CMCC-ESM2	Centro Euro-Mediterraneo sui Cambiamenti Climatici	Italy
GFDL-CM4	NOAA	USA
GFDL-ESM4	NOAA	USA

2.2. METHODOLOGY

2.2.1. Climate Model Selection

The process starts with extracting the outputs of GCMs for the given location and time period and this has been performed with the help of CDO (Climate Data Operator) [38]. Since all the climate models are in coarse resolution, spatial downscaling was performed assuming the outputs of GCM as grid points [39]. The Inverse Distance Weighting (IDW) was used to downscale four surrounding grid points of GCMs outputs to the observed station. The entire comparison between the outputs of GCMs to observed data is based on spatially averaged values for the sub-basin. For spatial averaging of station point data, the Thiessen polygon technique is applied.

The intention of the methodologies applied here mainly depends on displaying the very important characters of the climate time series which play a critical role in climate impact studies. So, based on the intensive literature review done on current methodologies applied and also the objective of this paper, a combination of methodologies are used. The selection or evaluation is based on historical/observed data and will be performed at four-time steps or levels which are monthly, seasonal (JJAS and MAM), and annual. This is to grasp all statistical characteristics of the time series. The selection will be done on climate models before bias correction, so that not to introduce bias into selection process.

In total, a combination of five methodologies has been applied which highlight the various characteristics of the time series. The first technique tries to fit a probability distribution to all climatic variables and checks which climatic models have a similar distribution to the observed climate variable. This was performed using the gamlss package [40] under R programming software [41]. The result of the distribution analysis was evaluated between the observed and climate models series using Akaike's Information Criterion (AIC). Then the climate model or models which have similar distribution is/are assumed to be the model/s that is/are capable of better describing the observed series.

The second technique observes the trend using the Mann - Kendall (MK) test [42,43]. In detecting the trend MK test calculates the statistic 'S' by ranking the data and calculating the sign as described in Equation (1) [42].

$$S = \sum_{i=1}^{n-1} \sum_{j=i+1}^{n} sgn(x_j - x_i) \quad (1)$$

Where: x_j - is data ranked from i = 1, 2, 3, . . . , n-1 and x_i- is the data ranked from j = i+1, 2, . . . , n

The sign is the difference between the original data x_i, shortened by one data point, and the data itself without the first data point x_j.

Preprints (www.preprints.org) | NOT PEER-REVIEWED | Posted: 7 September 2022 doi:10.20944/preprints202209.0108.v1

$$sgn(x_j - x_i) = \begin{cases} +1\ if(x_j - x_i) > 0 \\ 0\ if(x_j - x_i) = 0 \\ -1\ if(x_j - x_i) < 0 \end{cases} \quad (2)$$

It is observed that when the data point (observation) is more (n $\geq$ 10), the statistic 'S' becomes normally distributed with mean (E(S)) equal to zero and variance calculated as follows:

$$Var(S) = \frac{n(n-1)(2n+5) - \sum_{t=1}^{m} t_1(t_1-1)(2t_1+5)}{18} \quad (3)$$

Where: n - is the number of data points and t_i are the ties of the sample data series. The test statistic (Z_c) is calculated as:

$$Z_c = \begin{cases} \frac{S-1}{\sigma}\ if\ S > 0 \\ 0\ if\ S = 0 \\ \frac{S+1}{\sigma}\ if\ S < 0 \end{cases} \quad (4)$$

Where: σ is standard deviation of the statistic 'S'. From this test statistic (Zc) was concluded, and a positive value indicates an upward trend while a negative value is contrary. According to [43], this approach works well for data where there is no significant correlation at lag 1, if there is a significant correlation at lag 1 the modified MK test is applied. The method calculates the significance of the trend by modifying the variance of MK test statistic ('S') by ESS (Effective Sample Size). The significance is determined based on the p-values at a significance level of 0.05. Therefore if the p-values are greater than 0.05, then we accept the null hypothesis of there is no significant trend in the data and if it is less than or equal the reverse is true.

In the third approach, four performance metrics were applied to identify which climate model/s had better simulated the observed series. The selected measures are Coefficient of Determination (R^2), Root Mean Squared Error (RMSE), Mean Absolute Error (MAE) and BIAS. The performance measures were each applied for all time steps. And then a rank is assigned to each model based on the magnitude of the performance measure. Models which had an overall good performance at all four-time steps would be identified by summing up the ranks at the corresponding time step and ranking again finally.

Another technique applies a time series clustering technique to identify which climate model was able to capture the stochastic process of the observed series much better. For this, the Integrated Periodogram algorithm developed by [44] is used in the TSclust package [45] under R. This data mining approach tries to group time series into clusters based on their Integrated Periodogram (d_{IP}) as a distance (dissimilarity) measure. The periodogram technique helps in setting the comparison to be in frequency domain and this enables to characterize each time series in terms of its underlying stochastic behavior. The dissimilarity measure is calculated using Equation (5) [44],

$$d_{IP}(X_T, Y_T) = \int_{-\pi}^{\pi} |F_{X_T}(\lambda) - F_{Y_T}(\lambda)|\, d\lambda \quad (5)$$

Where the normalized cumulative periodograms at each data point j are given by:

$$F_{X_T}(\lambda_j) = \frac{1}{C_{X_T}} \sum_{i=1}^{j} I_{X_T}(\lambda_i) \quad (6)$$

$$F_{Y_T}(\lambda_j) = \frac{1}{C_{Y_T}} \sum_{i=1}^{j} I_{Y_T}(\lambda_i) \quad (7)$$

The weights used for normalizing the periodograms are as shown below where m is the number of data points in the original data series:

 doi:10.20944/preprints202209.0108.v1

$$C_{X_T} = \sum_{i=1}^{m} I_{X_T}(\lambda_i) \tag{8}$$

$$C_{Y_T} = \sum_{i=1}^{m} I_{Y_T}(\lambda_i) \tag{9}$$

The periodograms calculated at each time stamp (k) of the observed series is given by:

$$I_{X_T}(\lambda_k) = \frac{1}{T}|\sum_{t=1}^{T} X_t e^{-i\lambda_k t}|^2 \tag{10}$$

$$I_{Y_T}(\lambda_k) = \frac{1}{T}|\sum_{t=1}^{T} Y_t e^{-i\lambda_k t}|^2 \tag{11}$$

Here $\lambda_K = \frac{2\pi k}{T}$ is the frequency component corresponding to the input data sequence k ($k = 1, 2, ..., n$). Where as $n = \frac{T-1}{2}$ depends on the total data length of the observed series(T). In addition, X_t and Y_t correspond to each pair of time series in which dissimilarity measure is to be calculated for. Also the term i in Equations (10) and (11) indicates the imaginary term from the Fourier transformation of each pair of series.

A pairwise matrix of dissimilarity measure can be produced from the above procedure at which clustering is performed using the Agglomerative Hierarchical Clustering technique under Tsclust package in R that applies hclust() function from **stats** package. The classification into a cluster group or merging between clusters is through complete linkage criteria [44].

Finally, to understand the relationship between the observed and other climate model series, a Principal Component Analysis (PCA) has been applied. PCA is a dimensionality reduction technique that transforms a large number of correlated variables into a much smaller uncorrelated variable called Principal Components (PCs) [46]. Here the 11 variables (1 observed + 10 Climate models) were displayed into two-dimensional axes called principal components (PCs). The original data points for each variable can be plotted into a two-dimensional space called a score plot. This is done by projecting all data points into those two PCs using the loading vectors obtained from the covariance matrix. Score plot shows that points closer to origin are closer to average, points near to each other are similar, and points further outwards are outliers. The correlation between each variable can be better viewed using a loading plot. This plot is obtained by plotting the eigenvectors and indicates the contribution of each loading to the PCs. The relative length of the vector indicates its contribution to each PC and the angle between the vectors indicates the similarity between the variables. That means if the angle between two adjacent loading vectors of variables is smaller then they are more correlated, if orthogonal not related, and if in reverse direction then they are negatively correlated. A combined plot of score plot and loading plot is known as a Bi-Plot [47].

2.2.2. Downscaling, Bias Correction and Future Scenarios

The outputs of GCMs have to be Downscaled and bias-corrected before applying them to real-world situations. This is mainly because outputs of climate models have biases due to imperfect conceptualization and parametrization, insufficient length of data records, quality of reference data sets, and insufficient spatial resolution [48,49].

Here both the precipitation and temperature stations are first downscaled to each ground stations shown in Table 1 using the IDW technique and later bias corrected using quantile matching (QM) approach. QM method which uses empirical CDF obtained from the actual observations and requires no assumption of the underlying distribution which makes it preferable and has been applied here to the climate model with a top rank [50]. All the bias correction in this study is performed under R with the help of the qmap package

Preprints (www.preprints.org) | NOT PEER-REVIEWED | Posted: 7 September 2022 doi:10.20944/preprints202209.0108.v1

[49] on the daily climate series. The theoretical assumption of QM to estimate the bias correction So, is shown in Equation (12) as follows:

$$x_f = F_f^{-1}(F_o(x)) \tag{12}$$

Where: x_f is value of bias corrected future climate variable, $F_o(x)$ is CDF of Observed variable, F_f^{-1} is inverse CDF of future GCM, and x is the value of the future GCM variable before bias correction.

Two future scenarios (SSP5-8.5 and SSP2-4.5) and two time periods, mid-century (2040-2069) and end of the century (2070-2099), are used to understand the future climate of the Upper Awash Basin. The two scenarios each consider worst and middle future conditions. The worst scenario is the upper boundary in terms of the range of scenarios available and it can be considered an update of RCP8.5 of CMIP5. The second one, which is SSP2-4.5, indicates the medium pathway for future increase in greenhouse gas emissions which is similar to RCP4.5 of CMIP5.

3. Results

3.1. Selection of Climate Model

All the methods used are selected to highlight the very important characteristics of a climate time series which could play a critical role in addressing future climate impact in the study area. The evaluation criteria are distribution fitting, trend analysis, performance measures, DTW based hierarchical clustering, and PCA analysis. A total of ten climate models as shown in Table 2 were identified initially based on the common availability of climate models for the three climatic variables (Precipitation, Maximum temperature, and Minimum temperature). The models are evaluated for their statistical characteristics based on five different evaluation criteria and on different time levels (monthly, monthly average, seasonal and annual).

3.1.1. Identification of Distribution

For the observed and climate models series the best possible distributions have been identified with the help of gamlss package in R [40]. For example for the precipitation data of monthly average, JJAS, MAM, and annual series the observed data were found to have Normal (NO), Logistic(LO), Gamble(GA) and Normal(NO) distributions respectively. The PDF and CDF plots for only monthly average precipitation series of both observed and climate models are shown in Figure 2 below.

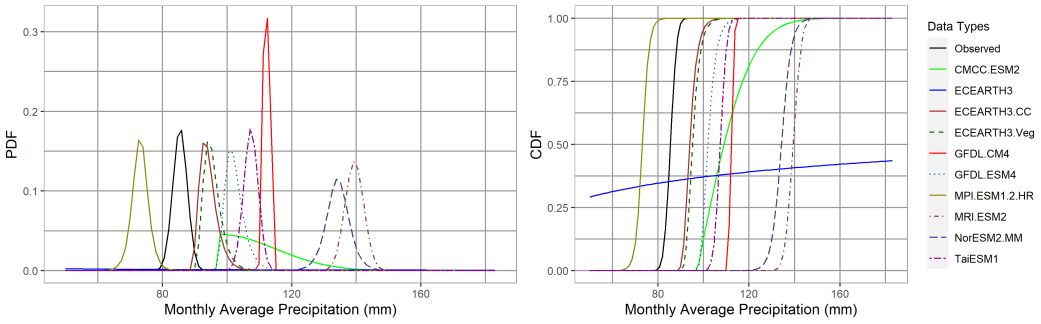

Figure 2. Fitted distribution for the monthly average precipitation (black line) series of the observed and 10 climate models (indicated with different colors).

The result of the distribution analysis for all three climatic variables and different time steps of analysis of both observed and climate models series is summarized in Table 3. For the precipitation series, it can be deduced that the MRI-ESM2-0 model was capable to have similar distributions with the observed series at all time steps except at MAM season. And TaiESM1 had similar distribution at Monthly and Annual time steps. Whereas

Preprints (www.preprints.org) | NOT PEER-REVIEWED | Posted: 7 September 2022 doi:10.20944/preprints202209.0108.v1

ECEARTH3-CC and NorESM2-MM had similar distributions only at MAM and JJAS seasons respectively.

In the case of the maximum temperature series, none of the climate models have shown a consistent similarity across different time steps as shown in Table 3. Here more than half of the models had similar distribution types at monthly average time step. Model MPI-ESM1-2-HR and ECEARTH3-Veg were able to have the same distribution with the observed series twice across those four time steps. And none of the models had similar distributions at the annual level. Few models have shared a similar distribution type with the observed series in the case of minimum temperature series. Here, only three models which are ECEARTH3, ECEARTH3-CC and MRI-ESM2-0 have shown similar distributions at JJAS, MAM, and Annual time steps respectively. There were no models which were capable of having similar distribution at the monthly average time step as shown in Table 3 below.

Table 3. Fitted Distributions for all three climatic variables across the four time steps of both observed and climate models series.

	Monthly Average		JJAS		MAM		Annual	
Data Type	AIC	DT	AIC	DT	AIC	DT	AIC	DT
Precipitation								
Observed	**221.62**	**NO**	**359.84**	**LO**	**348.147**	**GA**	**370.72**	**NO**
CMCC-ESM2	228.68	SN2	323.25	SEP1	356.37	SEP1	377.77	SN2
ECEARTH3	221.12	IGAMMA	355.27	WEI3	350.90	WEI	370.22	IGAMMA
ECEARTH3-CC	232.20	RG	346.75	NO	356.18	GA	381.30	RG
ECEARTH3-Veg	238.40	RG	343.27	NO	347.62	RG	387.50	RG
GFDL-CM4	230.72	SHASH	374.20	SEP1	366.36	WEI2	379.82	SHASH
GFDL-ESM4	241.38	RG	354.21	NO	349.64	WEI	390.47	RG
MPI-ESM1-2-HR	214.08	LO	348.57	WEI	335.65	RG	363.17	LO
MRI-ESM2-0	262.87	NO	375.29	LO	369.01	LOGNO2	411.96	NO
NorESM2-MM	253.75	LO	385.86	LO	387.26	WEI	402.84	LO
TaiESM1	223.07	NO	330.57	RG	351.91	LO	372.16	NO
Maximum Temperature								
Observed	**45.97**	**SN2**	**28.93**	**RG**	**51.31**	**WEI**	**13.19**	**PE2**
CMCC-ESM2	50.21	SN2	37.20	GT	59.44	SEP2	36.72	NO
ECEARTH3	52.76	SN2	41.46	NO	76.62	IGAMMA	39.00	IGAMMA
ECEARTH3-CC	51.94	SN2	44.98	SN2	64.69	GU	39.80	SN2
ECEARTH3-Veg	52.75	SN2	47.76	WEI3	65.84	WEI	38.94	IGAMMA
GFDL-CM4	48.37	IGAMMA	33.43	IGAMMA	57.72	RG	14.37	SN2
GFDL-ESM4	43.64	SEP2	40.69	NO	62.79	LO	31.29	SEP3
MPI-ESM1-2-HR	54.71	SN2	47.47	RG	67.22	WEI3	30.95	NO
MRI-ESM2-0	47.85	SEP2	40.41	LO	68.49	NET	23.92	RG
NorESM2-MM	44.26	RG	43.46	SN2	59.60	NO	31.55	SHASH
TaiESM1	56.18	SN2	20.05	WEI	56.78	NET	16.55	LO
Minimum Temperature								
Observed	**42.35**	**SEP1**	**30.9**	**NO**	**34.09**	**NO**	**16.98**	**IGAMMA**
CMCC-ESM2	47.79	SHASH	30.51	SEP1	55.5	IG	39.24	GT
ECEARTH3	38.80	SN2	29.41	NO	53.62	WEI	26.45	SN2
ECEARTH3-CC	35.67	SN2	34.40	LO	58.22	NO	31.58	WEI3
ECEARTH3-Veg	40.44	SN2	34.56	LO	58.99	SEP3	39.56	LO
GFDL-CM4	37.93	BCPEo	12.85	RG	43.25	RG	19.89	RG
GFDL-ESM4	49.12	GG	33.38	LO	55.99	IGAMMA	44.06	NO
MPI-ESM1-2-HR	51.99	SN2	22.69	RG	46.13	WEI3	29.87	SN2
MRI-ESM2-0	44.59	SN2	14.56	SN2	29.93	SEP2	36.91	IGAMMA
NorESM2-MM	44.07	SN2	23.15	GT	56.08	LO	49.61	SHASH
TaiESM1	48.96	BCPEo	25.77	NET	55.85	SN2	39.38	NET

NB: Those highlighted in grey are models that have shared the same distribution as observed time series across each time period of analysis. And DT means Distribution Type.

3.1.2. Trend Analysis

Trend analysis has also been performed similarly at four different levels same as in distribution analysis. For the precipitation series almost all of the models had similar trends as of observed series across all time steps except for three models at JJAS and one at MAM seasons which are not similar as shown in Table 4. These were models ECEARTH3, ECEARTH3-CC, and GFDL-ESM4 for the JJAS season and CMCC-ESM2 for MAM season.

For the maximum temperature series, ECEARTH3 does not have a similar trend to the observed series at any of the time steps. Three models (ECEarth3-CC, NorESM2-MM, and TaiESM1) were able to have a similar trend at three-time steps out of four. And EC-Earth3-Veg, GFDL-CM4, and MPI-ESM1-2-HR had similarities only at JJAS season as shown in

Preprints (www.preprints.org) | NOT PEER-REVIEWED | Posted: 7 September 2022 doi:10.20944/preprints202209.0108.v1

Table 4. Out of the ten models, MRI-ESM2-0 has shown similar trends across all four-time steps. Furthermore, among the ten models, GFDL-ESM4, MPI-ESM1-2-HR, NorESM2-MM, and TaiESM1 have similar trends to the observed minimum temperature series across all time steps whereas models CMCC-ESM2, ECEARTH3, GFDL-CM4, and MRI-ESM2-0 were the least. Two models ECEARTH3-CC and ECEARTH-Veg were able to have similarity at all time steps except for JJAS season as shown in Table 4.

Table 4. Results of Trend Analysis for all three climatic variables across the four time steps for both observed and climate models series.

Data Type	Annual		Monthly Ave.		JJAS		MAM	
	TTR	Direc	TTR	Direc	TTR	Direc	TTR	Direc
Precipitation								
Observed	**NS**	**-**	**NS**	**-**	**NS**	**-**	**NS**	**-**
CMCC-ESM2	NS	-	NS	-	NS	-	S	I
ECEARTH3	NS	-	NS	-	S	I	NS	-
ECEARTH3-CC	NS	-	NS	-	S	I	NS	-
ECEARTH3-Veg	NS	-	NS	-	NS	-	NS	-
GFDL-CM4	NS	-	NS	-	NS	-	NS	-
GFDL-ESM4	NS	-	NS	-	S	D	NS	-
MPI-ESM1-2-HR	NS	-	NS	-	NS	-	NS	-
MRI-ESM2-0	NS	-	NS	-	NS	-	NS	-
NorESM2-MM	NS	-	NS	-	NS	-	NS	-
TaiESM1	NS	-	NS	-	NS	-	NS	-
Maximum Temperature								
Observed	**S**	**I**	**S**	**I**	**NS**	**-**	**S**	**I**
CMCC-ESM2	S	I	S	I	S	I	NS	-
ECEARTH3	NS	-	NS	-	S	I	NS	-
ECEARTH3-CC	S	I	S	I	NS	-	NS	-
ECEARTH3-Veg	NS	-	NS	-	NS	-	NS	-
GFDL-CM4	NS	-	NS	-	NS	-	NS	-
GFDL-ESM4	S	I	S	I	S	I	NS	-
MPI-ESM1-2-HR	NS	-	NS	-	NS	-	NS	-
MRI-ESM2-0	S	I	S	I	NS	-	S	I
NorESM2-MM	S	I	S	I	NS	-	NS	-
TaiESM1	S	I	S	I	NS	-	NS	-
Minimum Temperature								
Observed	**NS**	**-**	**NS**	**-**	**S**	**I**	**NS**	**-**
CMCC-ESM2	S	I	S	I	S	I	S	I
ECEARTH3	S	I	S	I	NS	-	NS	-
ECEARTH3-CC	NS	-	NS	-	NS	-	NS	-
ECEARTH3-Veg	NS	-	NS	-	NS	-	NS	-
GFDL-CM4	S	I	S	I	S	I	S	I
GFDL-ESM4	NS	-	NS	-	S	I	NS	-
MPI-ESM1-2-HR	NS	-	NS	-	S	I	NS	-
MRI-ESM2-0	S	I	S	I	S	I	S	I
NorESM2-MM	NS	-	NS	-	S	I	NS	-
TaiESM1	NS	-	NS	-	S	I	NS	-

NB: NS(Not Significant),S(significant),I(Increasing),D(Decreasing),TTR(Trend Test Result), Direc (Direction)

3.1.3. Performance Measures

Four different performance indicators were implemented to identify models having good prediction capabilities across all time steps. Table 5 shows the summarized results of each model across those four time steps against four performance measures. The ranking

Preprints (www.preprints.org) | NOT PEER-REVIEWED | Posted: 7 September 2022 doi:10.20944/preprints202209.0108.v1

shown in the summary table for each performance measure was obtained by ranking the sum of ranks across time steps.

In the precipitation series, NorESM2-MM is the model which had a relatively poor overall performance in predicting the observed series. And it can be concluded that ECEARTH3 family are top performing ones since all are ranked in top half. For case of maximum temperature series, the GFDL-CM4 model has performed poorly and MPI-ESM1-2-HR is the top ranked model in terms of simulating the observed series as shown in the summary Table 5 below. From Table 5 it can also be observed that TaiESM1 and NorESM2-MM are models which has performed good and poorly in simulating the observed minimum temperature series respectively.

Table 5. Summary of model performances for all three climatic variables across four performance measures for both observed and climate models series.

	Ranks				
Data Type	R^2	RMSE	MAE	BIAS	Sum of Rank
Precipitation					
ECEARTH3-CC	1	3	3	3	10
ECEARTH3	6	1	2	2	11
MPI-ESM1-2-HR	7	2	1	1	11
ECEARTH3-Veg	10	4	4	5	23
GFDL-ESM4	9	5	5	4	23
TaiESM1	5	6	6	6	23
GFDL-CM4	3	7	7	7	24
CMCC-ESM2	2	8	8	8	26
MRI-ESM2-0	4	10	10	10	34
NorESM2-MM	8	9	9	9	35
Maximum Temperature					
MPI-ESM1-2-HR	6	1	1	1	9
ECEARTH3-CC	2	3	3	3	11
ECEARTH3	1	4	4	4	13
CMCC-ESM2	10	2	2	2	16
ECEARTH3-Veg	7	5	6	6	24
MRI-ESM2-0	8	6	5	5	24
TaiESM1	5	8	8	8	29
GFDL-ESM4	3	9	9	9	30
NorESM2-MM	9	7	7	7	30
GFDL-CM4	4	10	10	10	34
Minimum Temperature					
TaiESM1	3	2	2	2	9
ECEARTH3-Veg	2	4	4	1	11
GFDL-CM4	5	1	1	8	15
GFDL-ESM4	6	3	3	3	15
ECEARTH3	8	5	5	5	23
ECEARTH3-CC	9	6	6	4	25
MPI-ESM1-2-HR	1	8	8	9	26
CMCC-ESM2	4	10	10	6	30
MRI-ESM2-0	10	7	7	7	31
NorESM2-MM	7	9	9	10	35

3.1.4. Time Series Clustering

A time-series clustering technique is used in order to identify which climate model is better capable of simulating the observed series in terms of capturing the seasonal variation. This technique uses a distance measure calculated from the cumulative periodograms of the observed and climate models. Using the distance matrix calculated from the integrated

Preprints (www.preprints.org) | NOT PEER-REVIEWED | Posted: 7 September 2022 doi:10.20944/preprints202209.0108.v1

periodograms a complete link agglomerative hierarchical clustering was performed on the monthly precipitation, maximum and minimum temperature series.

From Figure 3 it can be observed that for the precipitation series those eleven models were clustered into four groups. And as expected models which come from the same modeling institution such as ECEARTH3 and GFDL families are clustered together. There is a clear separation in the dendrogram for the group which holds GFDL-ESM4, GFDL-CM4, and MRI-ESM2-0. This indicates these groups of models have less potential in simulating the seasonal behavior of the observed series. It can also be seen that the MPI-ESM1-2-HR model was able to be in the same cluster as the observed series. And the next in line in terms of having closer seasonal characteristics to the observed series is the ECEARTH3 families.

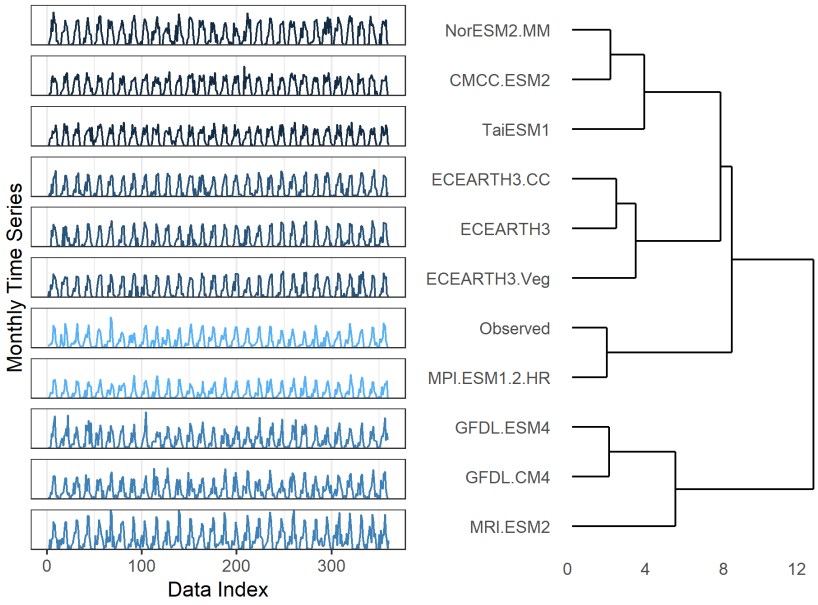

Figure 3. Clusters for monthly precipitation series for both observed and climate models series (Left figure: shows the cluster separation with blue color contrast, Right figure: grouping of climate models and observed data in terms of time series similarity based on seasonal pattern).

Similarly, for the monthly maximum temperature series, a clear clustering between models can be observed. Here the same models which are seen in the precipitation series are the ones that have similar seasonal characteristics as shown in Figure 4.

Preprints (www.preprints.org) | NOT PEER-REVIEWED | Posted: 7 September 2022 doi:10.20944/preprints202209.0108.v1

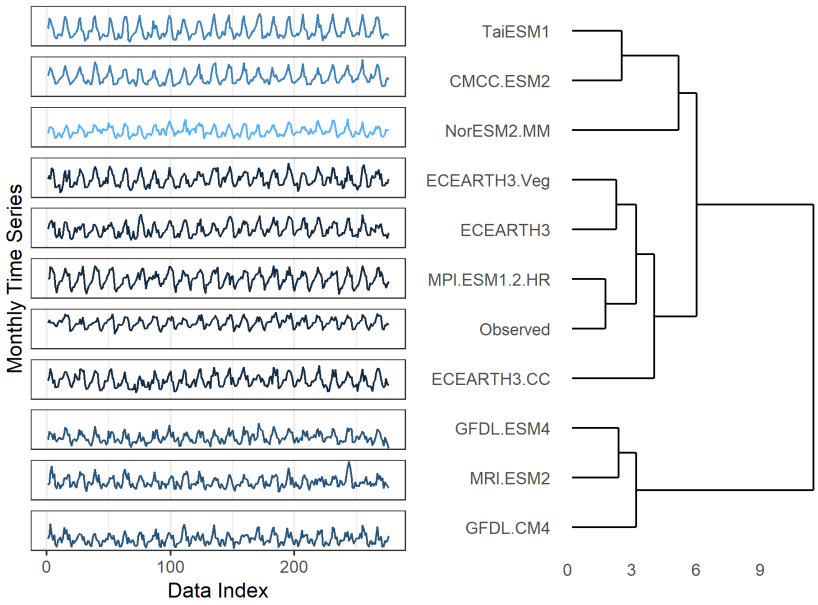

Figure 4. Clusters for monthly maximum temperature series for both observed and climate models series (Left figure: shows the cluster separation with blue color contrast, Right figure: grouping of climate models and observed data in terms of time series similarity based on seasonal pattern).

The clustering for the monthly minimum temperature series is different than the two previous cases as shown in Figure 5. Here the MRI-ESM2-0,CMCC-ESM2 and GFDL family has performed well in capturing the seasonal variation. Additionally, the dissimilarity between observed series and ECEARTH3 family and NorESM2-MM is relatively higher as compared to the rest of climate models.

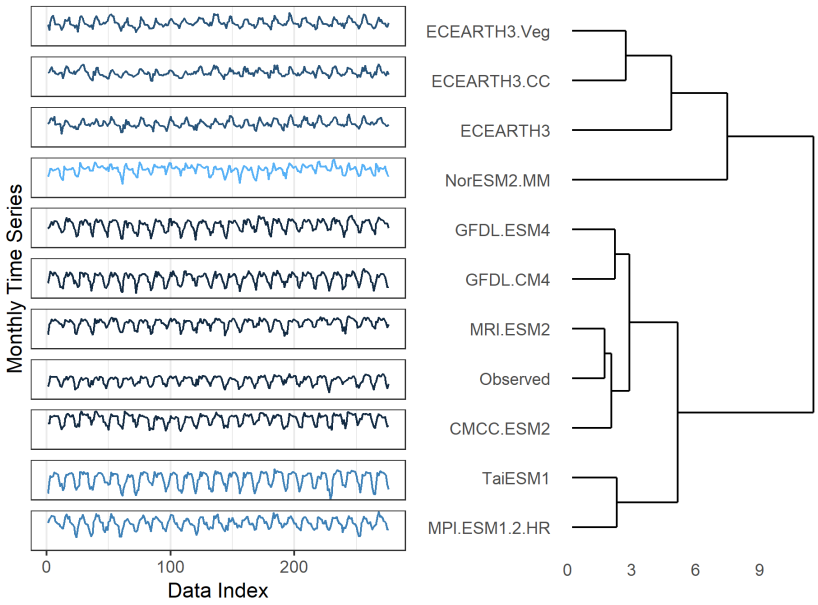

Figure 5. Clusters for monthly minimum temperature series for both observed and climate models series (Left figure: shows the cluster separation with blue color contrast, Right figure: grouping of climate models and observed data in terms of time series similarity based on seasonal pattern).

3.1.5. Principal Component Analysis (PCA)

From the PCA analysis of monthly precipitation data, most of the climate models are aligned along the PC1 with the exceptions of TaiESM1, CMCC-ESM2 and NorESM2-MM.

Preprints (www.preprints.org) | NOT PEER-REVIEWED | Posted: 7 September 2022 doi:10.20944/preprints202209.0108.v1

Nearly all of the variance of models ECEARTH3-Veg and ECAERTH3-CC is explained by PC1. Models MPI-ESM1-2-HR, ECEARTH3 and GFDL-ESM4 are one group that are closely correlated. As shown in Figure 6 the observed series is strongly correlated to GFDL-CM4.

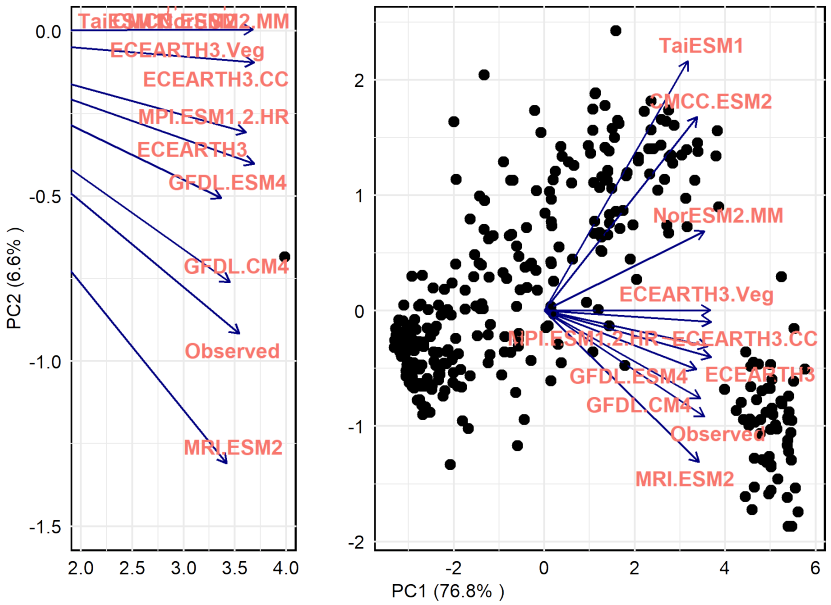

Figure 6. PCA Bi-plot for monthly precipitation series of both observed and climate model series. The Figure on the left is a zoomed out part of the main Bi-plot on the right.

All the ECEARTH3 families and GFDL-CM4 have shown a good correlation with observed maximum temperature series as shown in Figure 7. Where as the MRI-ESM2-0 and CMCC-ESM2 are the least correlated ones.

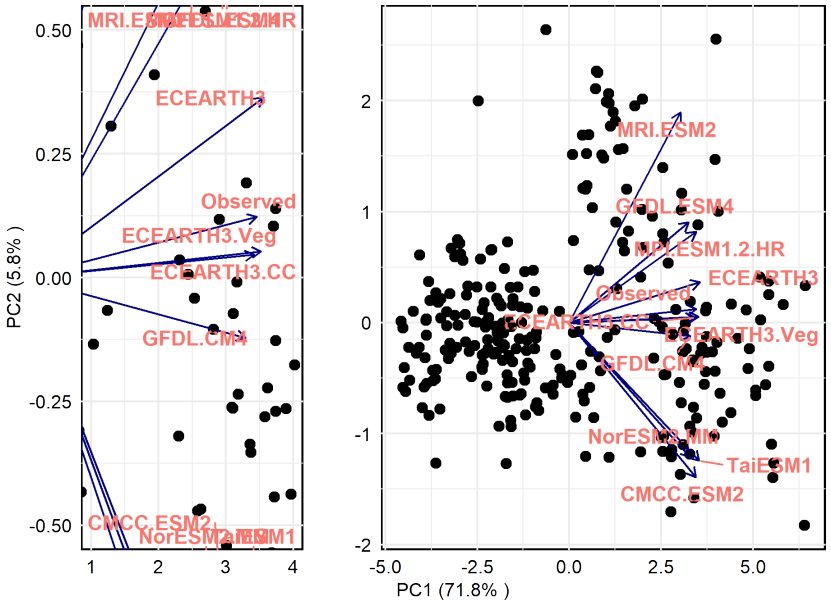

Figure 7. PCA Bi-plot for monthly maximum temperature series of both observed and climate model series. The Figure on the left is a zoomed out part of the main Bi-plot on the right.

On the contrary to the monthly maximum series, in the monthly minimum series the ECEARTH3 families have shown poor correlation. The most highly correlated model is GFDL-ESM4 and the second next best are groups of models which include CMCC-ESM2,GFDL-CM4 and MRI-ESM2-0 as shown in Figure 8.

Preprints (www.preprints.org) | NOT PEER-REVIEWED | Posted: 7 September 2022 doi:10.20944/preprints202209.0108.v1

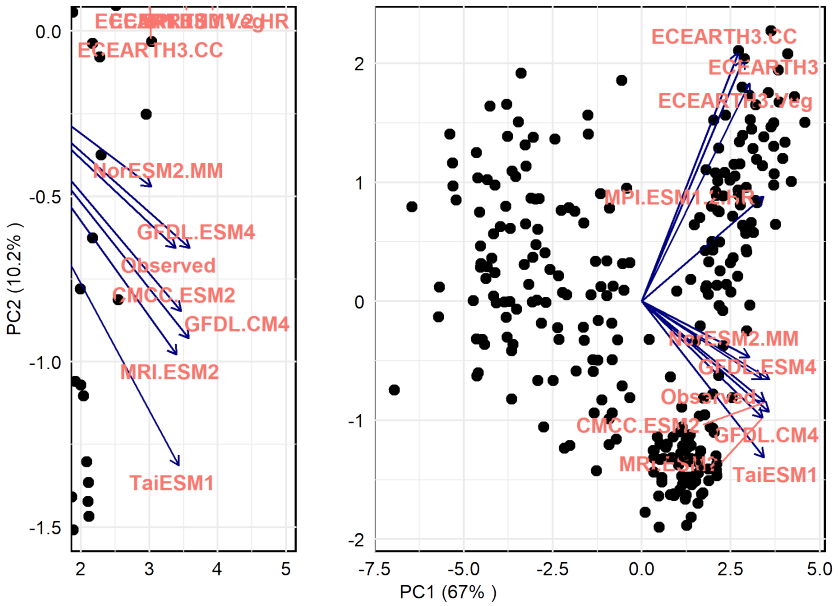

Figure 8. PCA Bi-plot for monthly minimum temperature series of both observed and climate model series. The Figure on the left is a zoomed out part of the main Bi-plot on the right.

3.2. Model Ranking and Interpretation

In the interpretation and summarization of all results, a simple rank-based system is used. Always a higher rank (lowest in terms of magnitude) would be given to a specific climate model for the desired effect. As an example in the interpretation of the result of distribution fitting if a specific model has been fitted with the same model as the observed series then a value of one(unit) would be assigned and if otherwise zero. Then these values would be summed across the four analysis periods for each model and given a rank. The ranking is from one to ten similar to the total number of climate models used in the study. A model would have a higher rank in this case if the sum of the value of the ranks is higher.

A similar approach is also used in the interpretation of trend analysis. That means if a similar trend is obtained for a specific model then a value of one is assigned and zero if on the contrary. The rest of the ranking procedure is the same as the one used in the interpretation of distribution analysis. For the case of the performance measure, a higher rank is given to a specific model that has scored well according to the criteria of each measure. Since four performance measures are used for each model the final was based on ranking the sum of ranks.

To interpret the cluster analysis the result of the distance (dissimilarity) matrix is used. A model with a minimum distance from the observed series is ranked higher than the one with a large distance. And finally, for the PCA analysis, the angle between the loading vectors of the observed and climate models is used as ranking criteria. Here similarly among those ten models, a model with less angle is much closer to the observed series so a higher-ranked would be assigned to it.

From the result of the precipitation time-series analysis across each method model CMCC-ESM2 has performed poorly as shown in Table 6. The top three models which have shown an overall good performance are MPI-ESM1-2-HR,MRI-ESM2, and ECEARTH3-CC.

Preprints (www.preprints.org) | NOT PEER-REVIEWED | Posted: 7 September 2022 doi:10.20944/preprints202209.0108.v1

Table 6. Summary rank based on five criteria used for evaluating the three climate model time series

Data Type	PDFR	TrendR	PMR	ClusterR	PCAR	SRank	FRank
Precipitation							
MPI-ESM1.2.HR	5	1	3	1	5	15	**1**
MRI-ESM2-0	1	1	9	5	3	19	**2**
ECEARTH3.CC	3	7	1	2	6	19	**2**
ECEARTH3	5	7	2	3	4	21	4
GFDL-CM4	5	1	7	10	1	24	5
ECEARTH3-Veg	5	1	4	8	7	25	6
TaiESM1	2	1	6	7	10	26	7
NorESM2-MM	3	1	10	4	8	26	7
GFDL-ESM4	5	7	5	9	2	28	9
CMCC-ESM2	5	7	8	6	9	35	10
Maximum Temperature							
ECEARTH3-CC	3	2	2	6	2	15	**1**
MPI-ESM1-2-HR	3	7	1	1	5	17	**2**
ECEARTH3-Veg	1	7	5	4	1	18	**3**
TaiESM1	3	2	7	2	7	21	4
ECEARTH3	7	10	3	3	3	26	5
NorESM2-MM	1	2	9	7	8	27	6
MRI-ESM2-0	3	1	6	8	10	28	7
CMCC-ESM2	7	5	4	5	9	30	8
GFDL-ESM4	7	5	8	9	6	35	9
GFDL-CM4	7	7	10	10	4	38	10
Minimum Temperature							
GFDL-ESM4	4	1	4	2	1	12	**1**
TaiESM1	4	1	1	6	6	18	**2**
MPI-ESM1-2-HR	4	1	7	3	7	22	**3**
GFDL-CM4	4	7	3	5	4	23	4
MRI-ESM2-0	1	7	9	1	5	23	4
CMCC-ESM2	4	7	8	4	3	26	6
ECEARTH3-Veg	4	5	2	7	8	26	6
NorESM2-MM	4	1	10	10	2	27	8
ECEARTH3	1	7	5	8	9	30	9
ECEARTH3-CC	1	5	6	9	10	31	10

NB: PDFR (PDF Rank), TrendR (Trend Rank),PMR (Performance Measure Rank), ClusterR (Custer Rank), PCAR (PCA Rank),SRank (Sum of Rank), FRank (Final Rank).

With the exception of the ECEARTH3-CC model the same two models had an overall good performance for the maximum temperature similar to the precipitation series as seen in Table 6. The least performance was observed for the GFDL family the same as before. In the case of the minimum temperature series the ECEARTH3 family has performed poorly and in contrary, the GFDL family are among the top performing as shown in Table 6.

Finally the same ranking methodology was applied to come into identification of possible models with an overall good performance for all three climatic variables of concern as shown in Table 7. It can be observed that the MPI-ESM1-2-HR model is one of the models with highest overall ranking when compared across the three climatic variables.

Preprints (www.preprints.org) | NOT PEER-REVIEWED | Posted: 7 September 2022 doi:10.20944/preprints202209.0108.v1

Table 7. Summary result for all three climatic variables

Data Type	Precip Rank	Tmax Rank	Tmin Rank	Sum of Rank	Final Rank
MPI-ESM1-2-HR	1	2	3	6	**1**
ECEARTH3-CC	2	1	10	13	**2**
TaiESM1	8	4	2	14	**3**
MRI-ESM2-0	3	7	4	14	**3**
ECEARTH3-Veg	6	3	6	15	5
ECEARTH3	4	5	9	18	6
GFDL-ESM4	9	9	1	19	7
GFDL-CM4	5	10	4	19	7
NorESM2-MM	7	6	8	21	9
CMCC-ESM2	10	8	6	24	10

3.3. Future Climate Projections

In order to say something about the future climate conditions in the study area QM technique was applied as a tool to bias correct the top-scoring climate model (MPI-ESM1-2-HR) for all three climate variables. In terms of the precipitation variable, for both time periods of analysis (mid and end of the century), a general increase in precipitation amount is observed. An increase of 6.5% and 4.7% in mean annual areal precipitation for the mid and end of a century respectively are observed for the middle scenario in the basin. Also for the worst-case scenario, an increment of 10.3% and 17.5% is seen for the mid and end of a century respectively.

The mean annual maximum temperature shows an increment of $1.5^{\circ}C$ and $2.2^{\circ}C$ for the mid and end of a century respectively in the middle scenario. With the same pattern, a rise of $2.6^{\circ}C$ and $3.5^{\circ}C$ for the mid and end of a century respectively is seen for the worst case. Similarly, for the minimum temperature series in the middle scenario an increase of $2.6^{\circ}C$ and $3.1^{\circ}C$ is observed for mid and end of a century respectively. The worst-case scenario showed an increment of $3.1^{\circ}C$ and $4.7^{\circ}C$ for mid and end of a century respectively.

4. Discussion

Models that are incorporated in the new CMIP6 archive have shown comparable or improved capability in terms of simulating the climate of the globe as compared to CMIP5 [51]. This is due to models in the CMIP6 archive are having improved model resolution, setup, scenarios, and parametrization than all previous CMIP versions [18]. This study has mainly focused on the application of statistical and data mining techniques to identify possible climate models from the new CMIP6 archive which can simulate the climate system of UASB. This was made possible after evaluating all those models against the observed historical climate series using those evaluation criteria. All comparison were performed on spatial averaged data for 1980 - 2009 period of analysis.

No specific model have shown consistent performance across each evaluation criteria and climatic variable as shown in Table 6. Model MRI-ESM2-0 was able to represent the distributional property for the precipitation and minimum temperature series. Where as EC-EARTH3-Veg for the maximum temperature series. In terms of capturing the trend behavior MRI-ESM2-0 was good for precipitation and maximum temperature series and models GFDL-ESM4, TaiESM1, MPI-ESM1-2-HR, and NorESM2-MM had equal potential for the minimum temperature series. Three different models represented each climate variable for their performance. These were EC-EARTH3 for precipitation, MPI-ESM1-2-HR for maximum temperature and TaiESM1 for minimum temperature. The seasonal pattern of precipitation and maximum temperature were better captured by MPI-ESM1-HR and for minimum temperature by MRI-ESM2-0. Not all three climate variables were correlated to the same climate model. GFDL-CM4,EC-EARTH3-Veg, and GFDL-ESM4 are models which had better correlation for precipitation, maximum temperature, and minimum temperature series respectively.

According to a recent study by [52] the summer rainfall over Ethiopia is influenced by SST condition over gulf of Guinea and southern Pacific ocean. Where as the spring rainfall is influenced by SST over north Atlantic ocean. Another work by [53] indicated that the rainfall season (JAS) climate system over the UASB is highly influenced by the

 doi:10.20944/preprints202209.0108.v1

equatorial pacific ocean temperature. ENSO and ITCZ that arise from the ocean temperature variations over equatorial pacific and low pressure zone near the equator are also another two important climate conditions that shapes the climate over UASB.

Most of the climate models evaluated in this study have different performance in terms of simulating this global climate processes. A recent work presented by [51] have shown that models EC-EARTH3, MPI-ESM1-2-HR and TaiESM1 do have good capabilities interms of capturing ENSO teleconnections. The model MPI-ESM1-2-Hr is also capable of producing the teleconnections over Indian and North Atlantic ocean reasonably well [54]. As shown in the result section this models are among the top ranked models in this study.

Another important reason why the top ranked model MPI-ESM1-2-HR has performed good may be due to the fact that it has higher atmospheric and ocean model resolution relative to those ten models. This model has 0.94° atmospheric resolution with 95 verticals and model top at 0.01hPa. And the ocean model is having 0.4° horizontal resolution with 40 levels [54,55]. Where as the least performed model which was CMCC-ESM2 has an atmospheric resolution of $0.9° \times 1.25°$ with 30 verticals and model top at 2hPa. And the ocean model is having a resolution of 0.33°[56]. Since topography of the study area is complex it is expected that model resolution plays a vital role in capturing all important climate characteristics of the study area.

Almost all of the climate modeling studies done so far on the basin have reported an expected increase in future temperature but a decrease in total precipitation especially for the end of the century [32–34,57]. However, both the previous AR5 and now the new AR6 IPCC reports predict that there will be an increase in annual mean precipitation and maximum temperature values for both mid and end of the century over East Africa [58,59]. So, it can be seen that the findings from these previous studies is in disagreement with the IPCC report. These fallacies may be due to the poor performance of these previous climate models in simulating the climate condition over East Africa or improper model selection. It can be observed that all of the findings of this study on future climate projections align with the new AR6 IPCC report of future climate condition over North-East Africa [59].

5. Conclusions

The outputs of the selection process have indicated that it is difficult to conclude on the performance of a single model since the performance of each model is different for each evaluation criteria. However, model MPI-ESM1-2-HR has shown an overall good performance when evaluated for all time steps and evaluation criteria.

When observing the outputs of each evaluation criteria across the three climatic variables, MRI-ESM2-0 model seems to be the best model with a more similar distribution (PDF) to the observed series. The second evaluation criteria for trend behavior shows that NorESM2-MM model was able to capture the trend well. The outputs of the performance measures (R^2,RMSE,MAE and BIAS) indicate that ECEARTH3-CC outperforms others. Also, MPI-ESM1-2-HR is best model in terms of capturing the stochastic behavior (underlying periodic patterns) of the observed series. And finally, the GFDL family was the model with highest correlation to the observed series.

Downscaling and bias correction for the top scoring MPI-ESM1-2-HR model for all three climate variables (Precipitation, Maximum temperature and Minimum temperature) were performed using IDW technique and QM approach. Based on the result of the downscaling and bias correction a prediction of future climate condition for two scenarios (middle and worst) and two centuries (mid and end) was done. The result of the future climate prediction for all three climate variables showed a positive relative increase as compared to the base period (1980-2009). And also the magnitude of increment is relatively higher for the end of century than mid century. All the outputs of this study are in agreement with new AR6 IPCC report about expected future climate changes on north east Africa.

The intensifying agricultural activity and urbanization in the study area [7] together with the projected increase in precipitation amount could increase the risk of flooding in the UASB in the future.

One of the limitation of these study is that only 10 climate models which are members of r1i1p1f1 ensemble are used in the identification of possible climate models. These were selected based on the commonality of the model outputs for all three climate variables under interest.

Author Contributions: Conceptualization, Y.A and T.A.; methodology, A.M.; software, Y.A.; validation, A.M., T.A. and Y.A.; formal analysis, Y.A.; investigation, Y.A.; resources, Y.A.; data curation, Y.A.; writing—original draft preparation, Y.A.; writing—review and editing, T.A.; visualization, Y.A.; supervision, A.M.; funding acquisition, A.M. All authors have read and agreed to the published version of the manuscript.

Funding: This research was funded by DAAD Home Grown Program 2019 and Universität der Bundeswehr München.

Data Availability Statement: All the data and analysis done is available upon request.

Acknowledgments: We would like to thank Ethiopian Meteorological Agency and WCRP (World Climate Research Program) for making the data available for research. And all those editors, reviewers and colleagues who have given their constructive comments in developing this manuscript.

Conflicts of Interest: The authors would like to declare there are no conflict of interest in the development of this manuscript.

References

1. Water, C. Leaving No One Behind. *The United Nations World Water Development Report* **2019**.
2. Gleick, P.H. *Water in crisis*; Vol. 100, New York: Oxford University Press, 1993.
3. Thakural, L.; Kumar, S.; Jain, S.K.; Ahmad, T. The impact of climate change on rainfall variability: a study in central himalayas. In *Climate Change Impacts*; Springer, 2018; pp. 181–192.
4. Shaaban, F.; Othman, A.; Habeebullah, T.M.; El-Saoud, W.A. An integrated GPR and geoinformatics approach for assessing potential risks of flash floods on high-voltage towers, Makkah, Saudi Arabia. *Environmental Earth Sciences* **2021**, *80*, 1–15.
5. Claire, S.; Denise, G. DroughtScape **2019**. pp. 3–6.
6. NMA. Climate Change National Adaptation Programme of Action (NAPA) of Ethiopia. *National Meteorological Services Agency (NMA), Ministry of Water Resources, Federal Democratic Republic of Ethiopia, Addis Ababa* **2007**.
7. Shawul, A.A.; Chakma, S. Spatiotemporal detection of land use/land cover change in the large basin using integrated approaches of remote sensing and GIS in the Upper Awash basin, Ethiopia. *Environmental Earth Sciences* **2019**, *78*, 1–13.
8. Nanesa, K. Awash River's the Ongoing Irrigation Practices, Future Projects and its Impacts on the Environment of Awash River Basin. *Irrigation Drainage Systems Engineering* **2021**, *10*.
9. Aregahegn, Z.; Zerihun, M. Study on Irrigation Water Quality in the Rift Valley Areas of Awash River Basin, Ethiopia. *Applied and Environmental Soil Science* **2021**, *2021*.
10. Mersha, A.N.; de Fraiture, C.; Masih, I.; Alamirew, T. Dilemmas of integrated water resources management implementation in the Awash River Basin, Ethiopia: irrigation development versus environmental flows. *Water and Environment Journal* **2021**, *35*, 402–416.
11. Edossa, D.C.; Babel, M.S.; Gupta, A.D. Drought analysis in the Awash river basin, Ethiopia. *Water resources management* **2010**, *24*, 1441–1460.
12. Shenduli, P.R.; Van Andel, S.J.; Mamo, S.; Masih, I. Improving hydrological prediction with global datasets: experiences with Brahmaputra, Upper Awash and Kaap catchments. *E-proceedings of the 37 th IAHR World Congress* **2017**.
13. Edwards, P.N. History of climate modeling. *Wiley Interdisciplinary Reviews: Climate Change* **2011**, *2*, 128–139.
14. Bhuvandas, N.; Timbadiya, P.V.; Patel, P.L.; Porey, P.D. Review of downscaling methods in climate change and their role in hydrological studies. *Int. J. Environ. Ecol. Geol. Mar. Eng* **2014**, *8*, 713–718.
15. Soriano, E.; Mediero, L.; Garijo, C. Selection of bias correction methods to assess the impact of climate change on flood frequency curves. *Water* **2019**, *11*, 2266.
16. Lutz, A.F.; ter Maat, H.W.; Biemans, H.; Shrestha, A.B.; Wester, P.; Immerzeel, W.W. Selecting representative climate models for climate change impact studies: an advanced envelope-based selection approach. *International Journal of Climatology* **2016**, *36*, 3988–4005.
17. Brief, C. How Do Climate Models Work?, 2018.
18. Ayugi, B.; Zhihong, J.; Zhu, H.; Ngoma, H.; Babaousmail, H.; Rizwan, K.; Dike, V. Comparison of CMIP6 and CMIP5 models in simulating mean and extreme precipitation over East Africa. *International Journal of Climatology* **2021**, *41*, 6474–6496.

19. Wilby, R. Evaluating climate model outputs for hydrological applications. *Hydrological Sciences Journal–Journal des Sciences Hydrologiques* **2010**, *55*, 1090–1093.
20. Khayyun, T.S.; Alwan, I.A.; Hayder, A.M. Selection of suitable precipitation CMIP-5 sets of GCMs for Iraq using a symmetrical uncertainty filter. In Proceedings of the IOP Conference Series: Materials Science and Engineering. IOP Publishing, 2020, Vol. 671, p. 012013.
21. Homsi, R.; Shiru, M.S.; Shahid, S.; Ismail, T.; Harun, S.B.; Al-Ansari, N.; Chau, K.W.; Yaseen, Z.M. Precipitation projection using a CMIP5 GCM ensemble model: a regional investigation of Syria. *Engineering Applications of Computational Fluid Mechanics* **2020**, *14*, 90–106, [https://doi.org/10.1080/19942060.2019.1683076]. https://doi.org/10.1080/19942060.2019.1683076.
22. Samadi, S.Z.; Sagareswar, G.; Tajiki, M. Comparison of general circulation models: methodology for selecting the best GCM in Kermanshah Synoptic Station, Iran. *International Journal of Global Warming* **2010**, *2*, 347–365.
23. Pitman, A.; Perkins, S.; et al. Reducing uncertainty in selecting climate models for hydrological impact assessments. *IAHS PUBLICATION* **2007**, *313*, 3.
24. Alemseged, T.H.; Tom, R. Evaluation of regional climate model simulations of rainfall over the Upper Blue Nile basin. *Atmospheric research* **2015**, *161*, 57–64.
25. Ongoma, V.; Chen, H.; Gao, C. Evaluation of CMIP5 twentieth century rainfall simulation over the equatorial East Africa. *Theoretical and Applied Climatology* **2019**, *135*, 893–910.
26. Nashwan, M.S.; Shahid, S. Symmetrical uncertainty and random forest for the evaluation of gridded precipitation and temperature data. *Atmospheric Research* **2019**, *230*, 104632.
27. Ahmadalipour, A.; Rana, A.; Moradkhani, H.; Sharma, A. Multi-criteria evaluation of CMIP5 GCMs for climate change impact analysis. *Theoretical and applied climatology* **2017**, *128*, 71–87.
28. Rana, A.; Madan, S.; Bengtsson, L. Performance evaluation of regional climate models (RCMs) in determining precipitation characteristics for Gothenburg, Sweden. *Hydrology Research* **2014**, *45*, 703–714.
29. Wilcke, R.A.; Bärring, L. Selecting regional climate scenarios for impact modelling studies. *Environmental Modelling & Software* **2016**, *78*, 191–201.
30. Srinivasa Raju, K.; Nagesh Kumar, D. Ranking general circulation models for India using TOPSIS. *Journal of Water and Climate Change* **2015**, *6*, 288–299.
31. Hailemariam, K. Impact of climate change on the water resources of Awash River Basin, Ethiopia. *Climate Research* **1999**, *12*, 91–96.
32. Taye, M.T.; Dyer, E.; Hirpa, F.A.; Charles, K. Climate change impact on water resources in the Awash basin, Ethiopia. *Water* **2018**, *10*, 1560.
33. Tadese, M.T.; Kumar, L.; Koech, R. Climate change projections in the Awash River Basin of Ethiopia using Global and Regional climate models. *International Journal of Climatology* **2020**, *40*, 3649–3666.
34. Daba, M.H.; You, S. Assessment of climate change impacts on river flow regimes in the upstream of Awash Basin, Ethiopia: based on IPCC fifth assessment report (AR5) climate change scenarios. *Hydrology* **2020**, *7*, 98.
35. Bussi, G.; Whitehead, P.G.; Jin, L.; Taye, M.T.; Dyer, E.; Hirpa, F.A.; Yimer, Y.A.; Charles, K.J. Impacts of Climate Change and Population Growth on River Nutrient Loads in a Data Scarce Region: The Upper Awash River (Ethiopia). *Sustainability* **2021**, *13*, 1254.
36. Emiru, N.C.; Recha, J.W.; Thompson, J.R.; Belay, A.; Aynekulu, E.; Manyevere, A.; Demissie, T.D.; Osano, P.M.; Hussein, J.; Molla, M.B.; et al. Impact of Climate Change on the Hydrology of the Upper Awash River Basin, Ethiopia. *Hydrology* **2022**, *9*, 3.
37. Gebresellase, S.H.; Wu, Z.; Xu, H.; Muhammad, W.I. Evaluation and selection of CMIP6 climate models in Upper Awash Basin (UBA), Ethiopia. *Theoretical and Applied Climatology* **2022**, pp. 1–27.
38. Schulzweida, U. CDO User Guide, 2021. https://doi.org/10.5281/zenodo.5614769.
39. Katz, R.W. Techniques for estimating uncertainty in climate change scenarios and impact studies. *Climate research* **2002**, *20*, 167–185.
40. Rigby, R.A.; Stasinopoulos, D.M. Generalized additive models for location, scale and shape,(with discussion). *Applied Statistics* **2005**, *54*, 507–554.
41. R Core Team. *R: A Language and Environment for Statistical Computing*. R Foundation for Statistical Computing, Vienna, Austria, 2021.
42. Mann, H.B. Nonparametric Tests Against Trend. *Econometrica* **1945**, *13*, 245–259.
43. Yue, S.; Wang, C. The Mann-Kendall test modified by effective sample size to detect trend in serially correlated hydrological series. *Water resources management* **2004**, *18*, 201–218.
44. De Lucas, D.C. Classification techniques for time series and functional data. PhD thesis, Universidad Carlos III de Madrid, 2010.
45. Montero, P.; Vilar, J.A. TSclust: An R Package for Time Series Clustering. *Journal of Statistical Software* **2014**, *62*, 1–43.
46. Kabacoff, R.I. *R in action: data analysis and graphics with R*; Manning Publishings Co., 2015.
47. Hartmann, K.; Krois, J.; Waske, B. E-Learning Project SOGA: Statistics and Geospatial Data Analysis. *Department of Earth Sciences, Freie Universitaet Berlin* **2018**, *33*.
48. Sarvina, Y.; Pluntke, T.; Bernhofer, C. COMPARING BIAS CORRECTION METHODS TO IMPROVE MODELLED PRECIPITATION EXTREMES. *Jurnal Meteorologi dan Geofisika* **2019**, *19*, 103–110.
49. Gudmundsson, L.; Bremnes, J.B.; Haugen, J.E.; Engen-Skaugen, T. Downscaling RCM precipitation to the station scale using statistical transformations–a comparison of methods. *Hydrology and Earth System Sciences* **2012**, *16*, 3383–3390.

50. Boé, J.; Terray, L.; Habets, F.; Martin, E. Statistical and dynamical downscaling of the Seine basin climate for hydro-meteorological studies. *International Journal of Climatology: A Journal of the Royal Meteorological Society* **2007**, *27*, 1643–1655.
51. Planton, Y.Y.; Guilyardi, E.; Wittenberg, A.T.; Lee, J.; Gleckler, P.J.; Bayr, T.; McGregor, S.; McPhaden, M.J.; Power, S.; Roehrig, R.; et al. Evaluating climate models with the CLIVAR 2020 ENSO metrics package. *Bulletin of the American Meteorological Society* **2021**, *102*, E193–E217.
52. Alhamshry, A.; Fenta, A.A.; Yasuda, H.; Kimura, R.; Shimizu, K. Seasonal rainfall variability in Ethiopia and its long-term link to global sea surface temperatures. *Water* **2020**, *12*, 55.
53. Taye, M.T.; Dyer, E.; Charles, K.J.; Hirons, L.C. Potential predictability of the Ethiopian summer rains: understanding local variations and their implications for water management decisions. *Science of the Total Environment* **2021**, *755*, 142604.
54. Jungclaus, J.; Fischer, N.; Haak, H.; Lohmann, K.; Marotzke, J.; Matei, D.; Mikolajewicz, U.; Notz, D.; Von Storch, J. Characteristics of the ocean simulations in the Max Planck Institute Ocean Model (MPIOM) the ocean component of the MPI-Earth system model. *Journal of Advances in Modeling Earth Systems* **2013**, *5*, 422–446.
55. Gutjahr, O.; Putrasahan, D.; Lohmann, K.; Jungclaus, J.H.; von Storch, J.S.; Brüggemann, N.; Haak, H.; Stössel, A. Max planck institute earth system model (MPI-ESM1. 2) for the high-resolution model intercomparison project (HighResMIP). *Geoscientific Model Development* **2019**, *12*, 3241–3281.
56. Cherchi, A.; Fogli, P.G.; Lovato, T.; Peano, D.; Iovino, D.; Gualdi, S.; Masina, S.; Scoccimarro, E.; Materia, S.; Bellucci, A.; et al. Global mean climate and main patterns of variability in the CMCC-CM2 coupled model. *Journal of Advances in Modeling Earth Systems* **2019**, *11*, 185–209.
57. Daba, Mekonnen, T.; Kassa, S.; Shemalis. Evaluating Potential Impacts of Climate Change on Surface Water Resource Availability of Upper Awash Sub-basin, Ethiopia rift valley basin. *Open Water Journal* **2015**, *3*.
58. Stocker, T.F.; Qin, D.; Plattner, G.K.; Tignor, M.; Allen, S.K.; Boschung, J.; Nauels, A.; Xia, Y.; Bex, B.; Midgley, B. IPCC, 2013: climate change 2013: the physical science basis. Contribution of working group I to the fifth assessment report of the intergovernmental panel on climate change, 2013.
59. Masson-Delmotte, V.; Zhai, P.; Pirani, A.; Connors, S.; Péan, C.; Berger, S.; Caud, N.; Chen, Y.; Goldfarb, L.; Gomis, M.; et al. Contribution of Working Group I to the Sixth Assessment Report of the Intergovernmental Panel on Climate Change, 2021.